A Domain-independent Dual-image based Robust Reversible Watermarking

Xuejing Guo[1], Yixiang Fang[1*], Junxiang Wang[1] ,Wenchao Zeng[1], Yi Zhao[1], Tianzhu Zhang[1] and Shi Yun-Qing[2]
[1]Jingdezhen Ceramic Instutute, Jingdezhen, 333000, China
[2]University of Pittsburgh, Pittsburgh, PA
[Email: fangyixiang@jci.edu.cn]
[*]Corresponding Author: Yixiang Fang.

Received April 4, 2022; accepted November 28, 2022; published December 31, 2022

Abstract

Robust reversible watermarking has attracted widespread attention in the field of information hiding in recent years. It should not only have robustness against attacks in transmission but also meet the reversibility of distortion-free transmission. According to our best knowledge, the most recent robust reversible watermarking methods adopt a single image as the carrier, which might lead to low efficiency in terms of carrier utilization. To address the issue, a novel dual-image robust reversible watermarking framework is proposed in this paper to effectively utilize the correlation between both carriers (namely dual images) and thus improve the efficiency of carrier utilization. In the dual-image robust reversible watermarking framework, a two-layer robust watermarking mechanism is designed to further improve the algorithm performances, i.e., embedding capacity and robustness. In addition, an optimization model is built to determine the parameters. Finally, the proposed framework is applied in different domains (namely domain-independent), i.e., Slantlet Transform and Singular Value Decomposition domain, and Zernike moments, respectively to demonstrate its effectiveness and generality. Experimental results demonstrate the superiority of the proposed dual-image robust reversible watermarking framework.

Keywords: Domain-independent, Dual-image, Reversible watermarking, Robust Watermarking

This work was supported by the National Natural Science Foundation of China under Grant 62063010, 62062044, 61762054 and science and technology project of Jingdezhen under Grant 2020ZDGG004. Many thanks to the anonymous reviewers for their insightful comments and valuable suggestions, which helped a lot to improve the paper quality. We express our thanks to Dr. Jin who checked our manuscript.

http://doi.org/10.3837/tiis.2022.12.014 **ISSN : 1976-7277**

1. Introduction

To protect the security of multimedia information such as information integrity, copyright protection, etc., digital watermarking is designed and widely utilized. In general, traditional digital watermarking might cause irreversible distortion to the cover image during the secret data hiding process. To solve this issue, reversible watermarking (RW) has been proposed [1], which could not only extract the hidden secret data but recover the cover image, which is significant for some specific fields such as medical and military fields.

So far, many RW methods have been proposed on a single image as the carrier and could be mainly divided into four categories, namely lossless compression based [2-3], histogram shifting based [4-9], difference expansion based [10-12] and prediction error expansion based [13-18]. Recently, in order to improve the utilization of carriers, dual-image RW is proposed. In dual-image RW schemes [19-25], the sender first duplicates the cover image to make two identical versions. Different secret information is then hidden into the above-mentioned identical versions to generate the corresponding two stego-images. The receiver could extract those secret data from both received stego-images and restore the cover image in the case of no attack is encountered.

However, most traditional RW methods [2-29] belong to fragile watermarking, which means the hidden secret data could not be completely extracted when some normal attacks are encountered, i.e., JPEG compression, Gaussian noise, and even malicious attacks. To solve this issue, robust reversible watermarking (RRW) is proposed, and its framework is shown in **Fig. 1**. When no attack occurs, RRW enables the receiver to extract the watermark and to recover the cover image. Otherwise, the hidden secret data could be fully extracted even if the reversibility is lost.

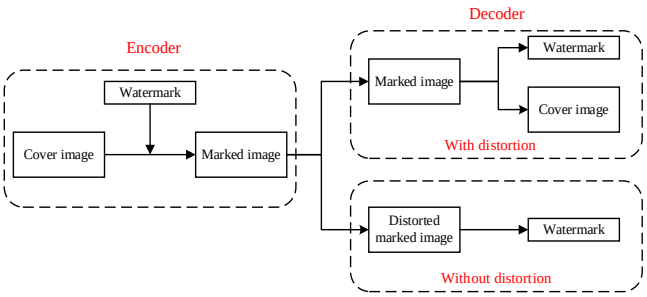

Fig. 1. RRW general framework

In recent years, several RRW schemes are proposed [30-42] based on a single image as the carrier, which could mainly be classified into three categories: (1) histogram rotation (HR) based schemes [30-31], (2) schemes based on the modifications of traditional HS [32-33], (3) two-stage RRW framework based schemes [34-42]. The HR based methods [30, 31] accomplish robust lossless watermarking by slightly rotating the centroid vectors of two random regions in the non-overlapping blocks. It was reported that these methods are robust to resist JPEG compression but are sensitive to “salt-and-pepper” noise. To solve the problem, schemes [32-33] based on a large modification of traditional HS can achieve good robustness. The method proposed by Zeng et al. in [32] divides the cover image into blocks and then exploits the arithmetic difference of each block to create the histogram. Gao et al. extended

Zeng's scheme by using a more efficient statistical quantity histogram [33]. For the third category, a two-stage general framework for RRW is proposed by Coltuc et al. [35-36]. The watermark is embedded into the cover image robustly in the first stage to generate an intermediate image. In the second stage, the information for recovery is embedded into the intermediate image by a reversible watermarking method. An et al. proposed a method based on a large modification of traditional HS in the wavelet domain [38]. In [38], the cover image would be divided into non-overlapping blocks and transformed into another domain to collect the coefficients. Then the watermark would be embedded into the coefficients by using histogram shifting. To improve the robustness, many two-stage RRW framework based schemes are developed in some transform domains and other domains such as the geometrical moment. Some discrete cosine transform domain (DCT) based RRW methods [35]-[36] are proposed to embed the secret data by modifying their frequency coefficients. In addition, the Slantlet transform domain (SLT) is used for RRW since it provides an optimal trade-off between time localization and smoothness characteristics [41]. Recently, Liu et al. proposed an RRW scheme based on SLT-SVD [34]. The method could further increase the robustness of the watermark by combining the SLT and the singular values decomposition (SVD). To improve the robustness for resisting most geometric attacks (e.g., rotation and scaling), Hu et al. proposed novel RRW schemes [37,39] to achieve the robustness to resist the geometric attacks by employing the polar harmonic transform (PHT) and Zernike moments (ZMs).
Because the embedding phases of the two stages are performed on the same domain, the watermark would be influenced by the reversible embedding stage. In [40], Wang et al. proposed a method to address the above-mentioned problem by using an independent domain.

However, it is observed that most robust reversible watermarking methods are performed on a single image. Inspired by dual-image RW [25], a novel dual-image RRW scheme is proposed in this paper to effectively exploit the correlation of dual images to achieve better algorithm performances, i.e., high visual quality of stego-image and large embedding capability. The main contributions of the proposed scheme are summarized as follows.

1. A novel dual-image RRW (denoted as DIRRW) framework is proposed.
2. A two-layer robust watermarking mechanism is designed in the proposed DIRRW framework to further improve the algorithm performances.
3. An optimization model is developed by optimizing the parameter.
4. Proposed framework, namely DIRRW is applied in different domains, i.e., SLT-SVD and Zernike domains, respectively to demonstrate its effectiveness and generality.

The rest of this paper is organized as follows. Section 2 briefs the related works for readers to better understand the proposed framework. The proposed method is presented in Section 3. Experimental results compared with some state-of-the-art RRW methods are reported in Section 4. Finally, we conclude this paper in the last section.

2. Related Works

In this section, we briefly introduce some related works in the following subsections. First, a two-stage RRW framework is introduced, which is the basis of our proposed framework. Then, a robust quantization index modulation watermarking algorithm [43] is briefly described.

2.1 Two-stage RRW framework

The two-stage general framework proposed by Coltuc et al in [35] and [40] is widely used in RRW methods. As shown in **Fig. 2**, the framework consists of two stages, namely the robust embedding stage and the reversible embedding stage. In the first stage, a watermark is

embedded into the cover image by using a robust embedding method to create the robust image (also called the intermediate image).

After that, in the second stage, the distortion produced by the robust embedding stage will be collected and then reversibly hidden into the robust image to generate the final stego-image.

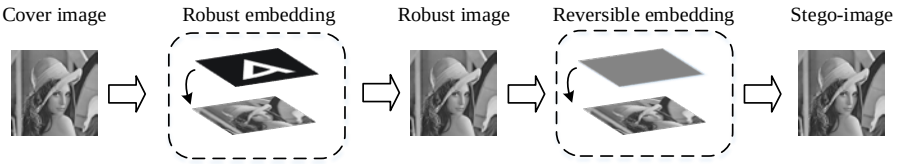

Fig. 2. Two-stage RRW framework

2.2 A classical quantization index modulation watermarking algorithm

A classical robust watermarking algorithm, namely Quantization Index Modulation (QIM) watermarking algorithm, is introduced in [43]. Specifically, the secret data embedding phase and extraction operation are calculated as follows.

1) Secret data embedding:

$$e' = \begin{cases} P * round(e/P) + P/2, & if\ mod(round(e/P), 2) = w \\ P * round(e/P) - P/2, & if\ mod(round(e/P), 2) \neq w \end{cases} \quad (1)$$

where quantization step length P is the threshold to control the robustness, $round(\cdot)$ is the rounded operation, and $mod(\cdot)$ indicates the modular operation. e indicates the original value and e' is the value embedded with the secret data w.

2) Secret data extraction:

The secret data w_i could be extracted in the decoder by (2)

$$w_i = mod(\lfloor E_i/P \rfloor, 2), \quad i = 1,2 \quad (2)$$

where $\lfloor \cdot \rfloor$ indicates the floor function.

Then, an example is taken to further illustrate the algorithm [43] as shown in **Fig. 3**.

Embedding phase: The quantization step length P is set to be 10, and the low-frequency coefficient is considered as $e \in (55,65)\ or\ (65,75)$. As shown in **Fig. 3**, when 1-bit secret data $w \in \{0,1\}$ is embedded, e would be changed to e'. Specifically, for $e \in (55,65)$, $e' = 55$ is got when $w = 1$, while $e' = 65$ is obtained when $w = 0$. If e is in the range (65,75), $e' = 75$ is acquired when $w = 1$, while $e' = 65$ could be obtained when $w = 0$.

Extraction phase: After the embedding phase, we could easily extract the embedded secret data w according to (2). If the received e' is not distorted, $w = 1$ could be extracted from $e' = 55\ or\ 75$, while $w = 0$ could be extracted from $e' = 65$. It is noted that, even the distorted version of e' (denoted as $\tilde{e}'$) is received , the secret data could be correctly extracted. For example, $w = 0$ could be correctly extracted when $\tilde{e}' \in (60,70)$. Obviously, the length of the range (60,70) is equal to P, which means that the length robustness range to perfectly extract secret data is determined by P.

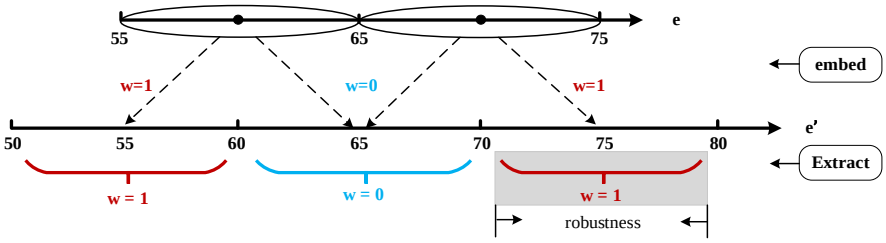

Fig. 3. Example of the embedding and extraction process of the QIM in [43]

3. Proposed Scheme

A novel dual-image RRW framework, denoted as DIRRW, is proposed in this section. The framework is established in Subsection 3.1. The algorithm for two-layer robust watermarking is then presented in Subsection 3.2. In Subsection 3.3, a theoretical analysis is offered by comparing the proposed scheme and classical schemes with a single image as the carrier. Finally, implementation details for the proposed scheme are mentioned in Subsection 3.4.

3.1 Proposed DIRRW framework

The proposed DIRRW framework is illustrated in **Fig. 4**. Two main parts are contained in the framework, i.e., robust embedding stage and reversible embedding stage.

Firstly, two duplicate images I_1 and I_2 are copied from the cover image I at the sender. Both I_1 and I_2 are then transformed into a certain domain, i.e., SLT-SVD or Zernike moments to collect the low-frequency coefficients for two channels. $E_1 = \{e_1^1, e_1^2, \cdots, e_1^{L/3}\}$ would be collected from the channel 1 (the channel where image I_1 is located). Similarly, $E_2 = \{e_2^1, e_2^2, \cdots, e_2^{L/3}\}$ would be collected from the channel 2.

Then, the L-length watermark W would be embedded into E_1 and E_2 by using the proposed two-layer robust watermarking algorithm, where W are divided into $W_i = \left\{w_i^1, w_i^2, \ldots, w_i^{L/3} | i = 1,2,3\right\}$. In detail, W_1 and W_2 would be embedded into E_1 and E_2 in the first layer. After that, $E_1' = \{e_1'^1, e_1'^2, \cdots, e_1'^{L/3}\}$ and $E_2' = \{e_2'^1, e_2'^2, \cdots, e_2'^{L/3}\}$ could be obtained, which would be modified to embed W_3 in the second layer by using their correlation. Last, $E_1'' = \{e_1''^1, e_1''^2, \cdots, e_1''^{L/3}\}$ and $E_2'' = \{e_2''^1, e_2''^2, \cdots, e_2''^{L/3}\}$ would be generated.

Later, the low-frequency coefficients sets E_1'' and E_2'' embedded with the secret data W would be utilized to replace the original sets E_1 and E_2. Then, two intermediate images I_{i1} and I_{i2} would be reconstructed by inversing the domain. Considering that the pixels in the constructed transition images and the final stego-images should be integers, I_{t1} and I_{t2} would be rounded to generate two robust images I_{r1} and I_{r2}.

To ensure the reversibility, the difference between the robust images and the cover image should be recorded as the auxiliary information H by referring to [37]. The auxiliary information consists of two parts, i.e., quantization errors occurred in the robust embedding phase (denoted as d_q) and rounded error occurred in the above-mentioned image rounded operation (denoted as d_r).

Finally, H would be hidden into the robust images I_{r1} and I_{r2} by employing the dual-image reversible data hiding method [25] to generate the final stego-images I_{w1} and I_{w2}.

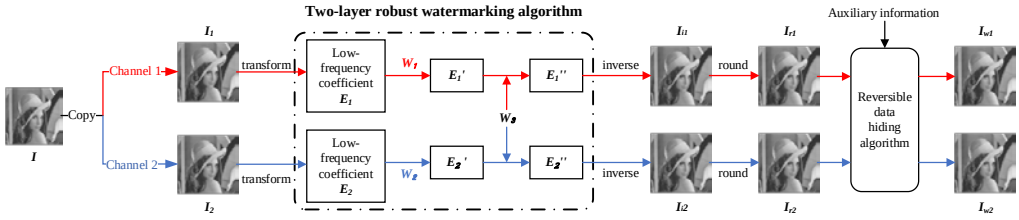

Fig. 4. Proposed dual-image RRW framework

In the case of no attack in the transmission, the cover image could be recovered and the watermark could be extracted at the decoder. In general, the auxiliary information H could be extracted from the stego-images I_{w1} and I_{w2} by referring to [25]. Meanwhile, the robust images I_{r1} and I_{r2} could be recovered. Later, the watermark W could be extracted from I_{r1} and I_{r2} and the cover image could be recovered from I_{r1} by using auxiliary information H. In the case of some attacks in the transmission, the reversibility is lost due to the vulnerability of the reversible embedding stage. However, the watermark W could be extracted directly from the distorted version of I_{w1} and I_{w2} due to the robustness of the two-layer robust watermarking algorithm in the proposed framework. The two-layer robust watermarking algorithm would be described in detail in the following subsection.

3.2 The two-layer robust watermarking algorithm

The proposed two-layer robust watermarking algorithm mentioned above would be utilized to embed the watermark W. After the embedding phases, the low-frequency coefficients E_1 and E_2 would be modified to $E_1''$and E_2''. The embedding and extraction processes would be introduced in detail as follows.

Embedding phase

In the first layer, the proposed algorithm is formed by mixing two advanced methods. As mentioned in Subsection 2.2, one is the QIM watermarking algorithm [43], which provides robustness for the embedding of the watermark. The other is the decimal preservation operation [37], which could reduce the cost of collecting auxiliary information before the reversible embedding stage.

Specifically, 1-bit secret data $w_1$and w_2 would be embedded into a pair of e_1 and e_2 utilizing the first-layer embedding algorithm by (3).

$$e_i' = \begin{cases} P * round(e_i/P) + P/2 + \Delta_i, & if\ mod(round(e_i/P), 2) = w_i \\ P * round(e_i/P) - P/2 + \Delta_i, & if\ mod(round(e_i/P), 2) \neq w_i \end{cases} \tag{3}$$

where P is the quantization step length as mentioned in Subsection 2.2, $\Delta_i = e_i - \lfloor e_i \rfloor$ is the decimal part of e_i. After the first layer embedding phase, e_1' and e_2' would be obtained. Meanwhile, d_q would be recorded via the first channel in our proposed scheme as follows:

$$d_q = e_1' - e_1 \tag{4}$$

In the second layer, the correlation between e_1' and e_2' could be exploited to provide a new space for further watermark embedding. In detail, two correlation coefficients are computed by (5).

$$\begin{cases} D = e_1' - e_2' \\ A = e_1' + e_2' \end{cases} \tag{5}$$

where D and A represent the difference and the sum of e_1' and e_2', respectively. Then, w_3 would be embedded by (6).

$$e_i'' = \begin{cases} e_i' + (-1)^i \frac{P}{4}, & if \ \ w_3 = mod(round(\frac{D}{P}),2) \\ e_i' - (-1)^i \frac{P}{4}, & if \ \ w_3 \neq mod(round(\frac{D}{P}),2) \end{cases} \tag{6}$$

After all of the watermark W are embedded, E_1'' and E_2'' would be obtained and be utilized to generate two robust images I_{r1} and I_{r2}.

Extraction and Recovery

If there is no attack during the transmission, the authorized users would receive two stego-images I_{w1} and I_{w2}. As mentioned in Subsection 3.1, auxiliary information $H = \{d_q \ d_r\}$ could be extracted at first, then the robust images I_{r1} and I_{r2} could be obtained. Then, E_1'' and E_2'' could be calculated. For each pair of e_1'' and e_2'', D' and A' could be calculated as follows:

$$\begin{cases} D' = e_1'' - e_2'' \\ A' = e_1'' + e_2'' \end{cases} \tag{7}$$

Then, the secret data w_3 could be extracted by (8).

$$w_3 = mod(round(\lceil D'/P \rceil),2) \tag{8}$$

where $\lceil \cdot \rceil$ means the rounded-up function. After that, e_1' and e_2' could be recovered as follows:

$$e_i' = \begin{cases} e_i'' + (-1)^i \frac{P}{4}, & if \ \ w_3 = mod(\left\lfloor \frac{A'}{P} \right\rfloor, 2) \\ e_i'' - (-1)^i \frac{P}{4}, & if \ \ w_3 \neq mod(\left\lfloor \frac{A'}{P} \right\rfloor, 2) \end{cases} \tag{9}$$

Later, w_1 and w_2 could be extracted by (2), and e_1 and e_2 could be recovered by (10).

$$e_1 = e_1' - d_q \tag{10}$$

As mentioned in Subsection 3.1, the cover image I could be recovered by using $E_1$and d_r in the end.

If the stego-images are distorted during transmission, the reversibility of the proposed method would be lost. However, the watermark W could be extracted correctly even if stego-images are slightly distorted due to the robustness of the proposed two-layer robust watermarking.

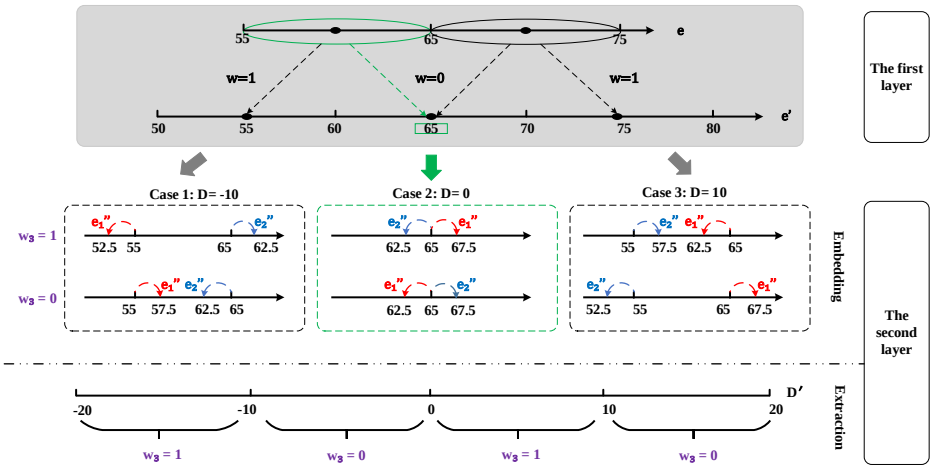

Fig. 5. Example of the embedding and extraction of the second layer

An example is shown in **Fig. 5** to further illustrate the embedding and the extraction procedures. Specifically, if e_1 and e_2 are both set to 60, both w_1 and w_2 are set to 0, and thus both e_1' and e_2' would be equal to 65 after the first layer embedding. Thus, D would be acquired as 0. If w_3 is equal to 1 in the second layer embedding process, e_1'' would be changed to 67.5, and e_2'' is changed to 62.5. Then, D' could be acquired to 5 and w_3 could be extracted to 1 at the receiver. After that, e_i' could be recovered to 65 by (9) and both w_1 and w_2 could be extracted to 0 by (2). It is noted that w_3 could be correctly extracted as long as D' is in the range of 0 to 10, which means that the robustness is similar to that of the first layer.

3.3 Theoretical analysis

In this subsection, the proposed scheme is analyzed to demonstrate its advantages from three aspects: embedding distortion (ED), embedding capacity (EC), and robustness.

On the one hand, the EDs of two typical QIM based robust watermarking algorithms are calculated. The ED of the QIM based watermarking algorithm [43] utilizing in the first layer of our proposed scheme is denoted as $Dis_{(1)}$ and calculated by (11).

$$Dis_{(1)} = \frac{\frac{1}{2}\int_a^{a+P}(x-a)^2 + (x-a-P)^2 dx}{P} = \frac{1}{3}P^2 \tag{11}$$

The ED of the QIM based [37] is expressed as $Dis_{(2)}$ and calculated as follows:

$$Dis_{(2)} = \frac{\frac{1}{2}\int_{a-\frac{P}{2}}^{a+\frac{P}{2}}(x-a)^2 + (x-a-P)^2\, dx}{P} = \frac{7}{12}P^2 \tag{12}$$

It is noted that $Dis_{(1)}$ is smaller than $Dis_{(2)}$ under the same value of P so that the less ED could be acquired in the former algorithm. On the other hand, the auxiliary information of an image would be compressed and then embedded into the robust image by using the method in [37]. While in our proposed DIRRW scheme, the auxiliary information H would be similarly collected from an image but embedded into two robust images by employing the method [25]. In other words, the auxiliary information embedded in each robust image in our proposed scheme is less than half of that in [37]. In summary, the better visual quality could be reached in our proposed scheme.

For EC, the EC_s of the watermarking methods in [37] and [43] are equal to $2L/3$ due to their single-channel property, while the EC of the proposed scheme could reach to L.

In addition, the robustness of our proposed two-layer embedding algorithm is equal to P as mentioned in Subsection 3.2. Noted that the large EC and the less ED could be accomplished in our proposed method. Thus, stronger robustness could be reached in our proposed scheme when the dual-image visual qualities are adjusted to be similar to that in the single-image RRW methods [37] and [43].

3.4 Implementation details

The encoding and decoding processes in the proposed scheme are designed. In addition, P would be optimized according to the user's needs to better control the robustness and visual effects.

Encoding Steps

Step1: The sender copies the original cover image I to generate two cover images I_1 and I_2. I_1 and I_2 are transformed into another domain (SLT-SVD or ZMs adopted in this paper). The methods for selecting low-frequency coefficients in the SLT-SVD domain and Zernike moments can be referred to [34] and [37]. Then, two sets of low-frequency coefficients E_1 and E_2 are collected for the robust watermarking.

Step2: In the proposed two-layer robust watermarking algorithm, secret data w_1 and w_2 are individually embedded into e_1 and e_2 during each channel by (3) in the first layer. Then, e_1' and e_2' are obtained.

Step3: The correlation between e_1' and e_2' is exploited and then modified to embed w_3 by (6) in the second layer. Later, e_1'' and e_2'' are obtained.

Step4: After the watermark W is fully embedded, E_1'' and E_2'' are utilized to reconstruct the intermediate images I_{i1} and I_{i2} as mentioned in Subsection 3.1. Subsequently, the robust images I_{r1} and I_{r2} are generated by rounding I_{i1} and I_{i2} to UINT8 data type.

Step5: Before the reversible embedding in this paper, d_q is collected by (4) and $d_r = I - \hat{I}_1$ is collected by referring to [37]. Afterwards, the auxiliary information $H = \{d_q\ d_r\}$ would be compressed and then embedded into the robust images I_{r1} and I_{r2} by using the dual-image reversible data hiding method [25]. In the end, the stego-images I_{w1} and I_{w2} are generated.

Optimization process: To optimize P , the robust embedding distortion (denoted as Dis) is devised in this paper as follows:

$$Dis = L\log_{10}\sqrt{\frac{1}{4}\int_{3P/2}^{5P/2}\left(x-\frac{5P}{4}\right)^2+\left(x-\frac{7P}{4}\right)^2+\left(x-\frac{9P}{4}\right)^2+\left(x-\frac{11P}{4}\right)^2 dx} \quad (13)$$

where L represents the length of the watermark. The optimization model of the parameter P could be expressed as follows:

$$\begin{cases} Max\ P \\ s.t. \\ \begin{cases} L = selected\ number \\ Dis \le k \end{cases} \end{cases} \quad (14)$$

Among them, k is a parameter determined by users. In this paper, L is set to 128 and P is optimized by exhaustive search in the set $\{1< P <50\}$ when the ZMs domain is selected. In general, the lowest peak signal-to-noise (PSNR) of the stego-image in a RRW method should be greater than 38dB to guarantee the visual quality. In this case, the experimental data k is set to 388. The optimized $P = 14$ is obtained by (14) when ZMs is chosen as the transform domain. Similarly, the optimized $P = 260$ is obtained when the SLT-SVD domain is selected.

Decoding Steps

1) Undistorted:

Step1: Extract the auxiliary information $H = \{d_q\ d_r\}$ and the robust images I_{r1} and I_{r2} could be recovered according to [25] in the meantime.

Step2: Transform I_{r1} and I_{r2} into the same domain which is selected in the encoding process. After that, the modified low-frequency coefficients sets E_1'' and E_2'' are obtained.

Step3: The secret data w_3 could be extracted according to (8) and both e_1' and e_2' could be recovered by (9).

Step4: The secret data w_1 and w_2 could be extracted according to (2). Meanwhile, e_1 could be restored with the quantized error d_q by (10).

Step5: Repeat the steps 3-4 of the decoding process until the watermark W is extracted completely. Then, the image $\hat{I}_1$ could be reconstructed by reversing E_1 into pixel domain. Finally, the original cover image I would be recovered by formula as follows:

$$I = \hat{I}_1 + d_r \tag{15}$$

2) Distorted:

The distorted stego-images $\tilde{I}_{w1}$ and $\tilde{I}_{w2}$ would be received at the decoder. The decoding steps in the case of distortion are similar to those in the undistorted case except- ing recover the original cover image. Although the reversibility is lost, the watermark W could be extracted due to the robustness of the proposed DIRRW scheme.

4. Experimental Results

In the section, the proposed method is evaluated by comparing with other three state-of-the-art methods, i.e., Liu et al.'s [34], Hu et al.'s [37] and Wang et al.'s [40], in terms of robustness and visual quality. In this paper, 100 typical $512 \times 512 \times 8$ bits grayscale images with different textures from the CVG-UGR and DIP databases [44, 45] are employed as test images, where some standard images are shown in **Fig. 6**. The methods in [34], [37] and [40] are all based on a single image as the carrier. Liu et al.'s method is based on the SLT-SVD domain. Hu et al.'s method is implemented in the Zernike moments (ZMs). Wang et al.'s method is a typical RRW that is based on an independent domain. To perform a fair comparison, the length L of the watermark in [34], [37] and [40] is set to 128. While the total embedding capacity is 256 bits in our proposed dual-image RRW method. Specifically, the size of non-overlapping blocks in Liu's method and the proposed SLT-SVD based dual-image RRW (denoted as SS-DIRRW) are set to 8×8. The parameters T =1000 and N =31 are set in Hu's method and the proposed Zernike moments dual-image RRW (denoted as ZMs-DIRRW). In [40], the block size is set to 64×16. P in the proposed SS-DIRRW and ZMs-DIRRW is the threshold to adjust the tradeoff between the robustness and perception for the stego-image, which means the larger P results in better robustness but worse visual quality for the stego-image, and vice versa. Similarly, the parameter Δ in [34] and [37], and ζ in [40] play the same role as P. The visual quality of the proposed scheme would be tested at first to indicate the visual difference between the dual images. PSNR is employed to measure the visual quality of the images, which is computed as follows:

$$PSNR = 10log_{10}\left(\frac{255^2 \times r \times c}{\sum_{i=1}^{r}\sum_{j=1}^{c}\left(I(x,y) - I_w(x,y)\right)^2}\right) \tag{16}$$

where r, c demotes the length and the width of the image, respectively. And x, y is the pixel coordinate of the image, respectively. I is the cover image and I_w is the stego-image.

Fig. 6. Four standard test images

Table 1. PSNRs of the dual stego-images in the proposed SS-DIRRW with P = 260 and in the proposed ZMs-DIRRW with P = 14

Method	Lena	Lake	Baboon	Boat	Average
SS-DIRRW	38.8	39.0	38.7	37.9	39.2
	39.5	38.8	38.4	38.9	39.2
ZMs-DIRRW	38.2	38.1	38.2	38.3	38.1
	38.4	38.2	38.5	38.0	38.2

By using the optimization model, P is optimized in the SLT-SVD and ZMs, respectively. Experientially, P is acquired to 260 in the proposed SS-DIRRW and is acquired to 14 in the proposed ZMs-RRW. The PSNRs of the dual stego-images (i.e., I_{w1} and I_{w2}) are listed in **Table 1**, in which $P = 260$ in the proposed SS-DIRRW and in the proposed ZMs-DIRRW with $P = 14$. It is observed that the PSNRs of the dual stego-images for the proposed methods are close to each other, whether in SLT-SVD or ZMs. Then, the smaller PSNRs of the dual stego-images in the proposed methods would be exploited in the following experiments of visual quality and robustness.

Table 2. PSNRs of [34], [37], the proposed SS-DIRRW and the proposed ZMs-DIRRW under the same level of the robust thresholds

Methods	Lena	Lake	Baboon	Boat	Average
[34]	34.1	35.2	35.5	34.7	33.7
SS-DIRRW	**38.8**	**38.8**	**38.8**	**37.9**	**39.2**
[37]	34.3	35.4	35.7	34.9	34.1
ZMs-DIRRW	**38.2**	**38.1**	**38.2**	**38.0**	**38.1**

4.1 Visual quality

In this subsection, PSNRs of [34], [37], the proposed SS-DIRRW and the proposed ZMs-DIRRW are under the same level of the robust thresholds and are listed in **Table 2**. In order to reach the same level of the robust thresholds, Δ in [34] and P in the proposed SS-DIRRW are set to 260, Δ in [37] is set to 28 and P in the proposed ZMs-DIRRW is set to 14. Under this condition, the proposed schemes (SS-DIRRW and ZMs-DIRRW) achieve better visual quality than the other traditional single-image RRW methods.

4.2 Robustness

The bit error rate (BER) is exploited to indicate the robustness of given schemes as follows:

$$BER = \frac{L_e}{L_o} \tag{17}$$

where L_e refers to the number of error secret data bits and L_o denotes the number of original secret data bits. The less BER is, the better robustness is achieved.

Geometric deformations (e.g., rotation and scaling) and common attacks (e.g., JPEG compression and Gaussian noise) would occur from time to time during the network transmission of the images. To testify the robustness performance, the experiments are performed between the proposed scheme and the other three state-of-the-art works, i.e., [34], [37] and [40], based on the above-mentioned test images in **Fig. 6**. In order to guarantee the visual quality of the stego-images, PSNRs of all the contract methods are adjusted to no less

than 38. Specifically, Δ=180 is set in [34], Δ =18 is set in [37] and ζ = 2.4 is set in [40]. Meanwhile, P =240 is set in our proposed SS-DIRRW and P =14 is set in the proposed ZMs-DIRRW which are optimized by our designed optimization model as mentioned in Section 3.

The robustness of the schemes is testified based on several types of attacks, i.e., rotation, scaling, JPEG compression, additive Gaussian noise and JPEG2000 compression. **Fig. 7** illustrates the five versions of the image Lena after the above different types of attacks.

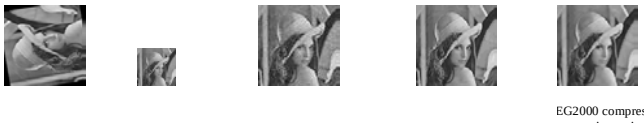

Fig. 7. The image Lena after being attacked

Since the stego-images I_{w1} and I_{w2} would be generated in our proposed methods (SS-DIRRW and ZMs-DIRRW), two cases are considered in the paper as follows: Case 1: *The Same Attacks* (I_{w1} and I_{w2} encounter the same attacks under this case). Case 2: *Different Attacks* (I_{w1} and I_{w2} suffer from different attacks).

Case 1: The Same Attacks.

The comparison between our proposed method (SS-DIRRW and ZMS-DIRRW) and the other three state-of-the-art works (i.e., [34], [37] and [40]) are performed under the above-mentioned five attacks and they are illustrated from **Fig. 8** to **Fig. 11**. As shown in **Fig. 8**, it is observed that the proposed ZMs-DIRRW achieves the same or even better robustness resistant to the geometric attacks especially the scaling attack when the factor is 0.6. This situation demonstrates the proposed DIRRW framework could significantly improve the robustness.

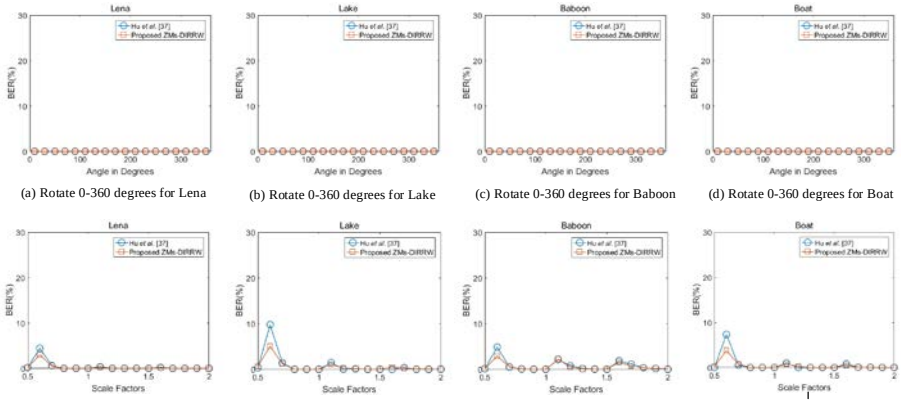

(a) Rotate 0-360 degrees for Lena (b) Rotate 0-360 degrees for Lake (c) Rotate 0-360 degrees for Baboon (d) Rotate 0-360 degrees for Boat

(a) Scale factor 0.5-2 for Lena (b) Scale factor 0.5-2-for Lake (c) Scale factor 0.5-2 for Baboon (d) Scale factor 0.5-2 for Boat

Fig. 8. Robustness to resist geometric attacks with [37]

It is observed that the BER of our proposed SS-DIRRW is less than which of [34] under the common attacks like JPEG compression, Gaussian noise and JPEG2000 compression. Similarly, the BER of the proposed ZMs-DIRRW is less than Hu's method [37]. In **Fig. 9**, the proposed SS-DIRRW achieves the least BER (<5%) at Gaussian noise with a variance of 0.029. The proposed ZMs-DIRRW achieve the similar experimental results when JPEG2000 compression reaches 100:1 for four standard test images. In addition, the results of the proposed methods (ZMs-DIRRW and SS-DIRRW) are excellent and stable. Even when the

quality factor is set to 10 in JPEG compression, all of the secret data are extracted without any errors in our proposed methods.

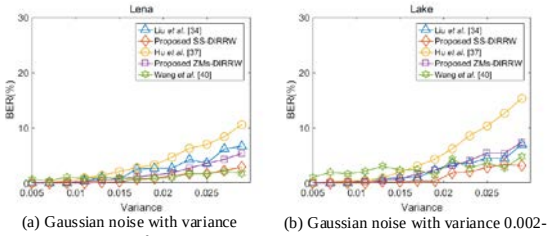

(a) Gaussian noise with variance 0.002-0.029 for Lena (b) Gaussian noise with variance 0.002-0.029 for Lake

(c) Gaussian noise with variance 0.002-0.029 for Baboon (d) Gaussian noise with variance 0.002-0.029 for Boat

Fig. 9. Robustness to resist additive gaussian noise compared with [34], [37] and [40]

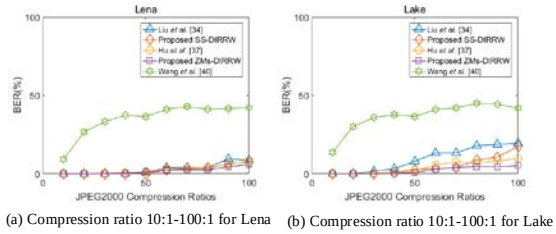

(a) Compression ratio 10:1-100:1 for Lena (b) Compression ratio 10:1-100:1 for Lake

(c) Compression ratio 10:1-100:1 for Baboon (d) Compression ratio 10:1-100:1 for Boat

Fig. 10. Robustness to resist JPEG2000 compression compared with [34], [37] and [40]

It is obviously that the robustness of the proposed SS-DIRRW and ZMs-DIRRW is slightly inferior to Wang's method [40] under the Gaussian noise with a variance of 0.029 for Lena and Baboon as shown in **Fig. 9**. However, for most cases, i.e., JPEG compression, JPEG2000 compression, rotation, and scaling, the robustness of the proposed schemes is superior to the other contrast schemes.

Besides the above-mentioned five attacks, some other common noise attacks such as medium and average filter operations are tested in the robustness experiment. The experimental results are shown in **Fig. 12**. The less BER of the proposed SS-DIRRW and ZMs-DIRRW further demonstrates the superiority of the proposed methods under the most common attacks.

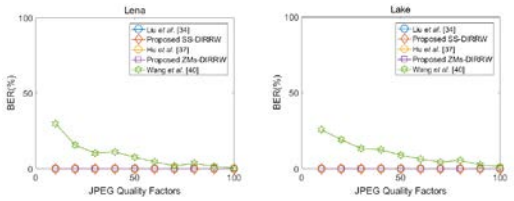

(a) Quality factor 10-100 for Lena (b) Quality factor 10-100 for for Lake

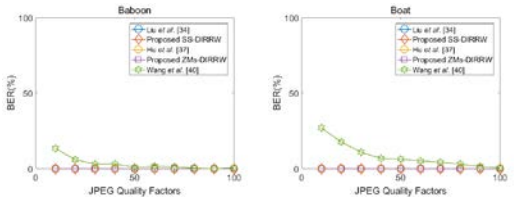

(c) Quality factor 10-100 for Baboon (d) Quality factor 10-100 for Boat

Fig. 11. Robustness to resist JPEG compression compared with [34], [37]and [40]

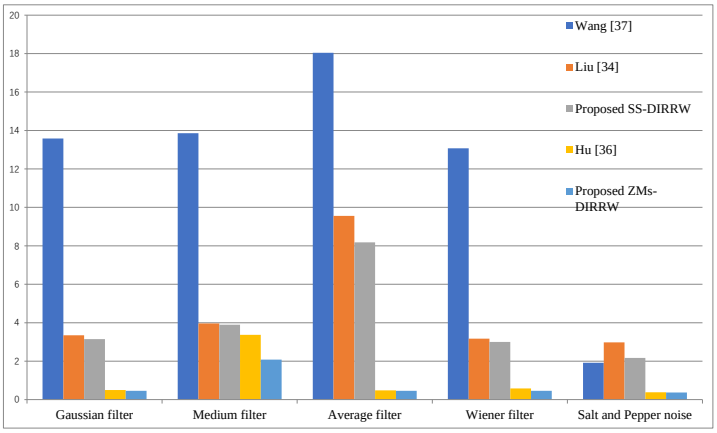

Fig. 12. The BERs for compared methods under other common noise attacks

Case 2*： *Different Attacks.

The proposed ZMs-DIRRW is taken for robustness test under this condition. Set several different kinds of attacks as follows: Rotation with angle 100, scaling with factor 0.5, gaussian noise with mean 0 and variance 0.02 and JPEG2000 compression with ratio 70:1. Six different attacks are performed on stego-images I_{w1} and I_{w2} to test the robustness under Case 2 and the result is listed in **Table 3**. Evidently, the excellent and comparable BERs of the ZMs-DIRRW are obtained under different attacks, which means similar robustness could be achieved regardless of Case 1 (same attacks) or Case 2 (different attacks). The phenomenon is attributed to the high utilization of the generated dual stego-images.

Table 3. BERs of the proposed ZMs-DIRRW under the different attacks

Image	Rotate100 Resize0.5	Rotate 100 Gaussian 0.02	Rotate 100 JPEG2000 70:1	Resize 0.5 Gaussian 0.02	Resize 0.5 JPEG2000 70:1	Gaussian 0.02 JPEG2000 70:1
Lena	0	0.39	0.47	0.63	0.78	3.13
Lake	0	0.63	1.33	1.33	1.88	3.20
Baboon	0	0.55	1.72	0.16	2.73	2.42
Boat	0	0.39	0.78	0.55	1.02	1.88
Average	**0**	**0.45**	**0.98**	**0.66**	**1.18**	**2.37**

5. Conclusion

In this paper, a novel dual-image based robust reversible watermarking framework is proposed. In addition, to further improve high performance, a two-layer robust quantization watermarking algorithm is designed. Meanwhile, both different domains are incorporated into the proposed framework to build two examples, i.e., SS-DIRRW and ZMs-DIRRW, to demonstrate its superiority. Experimental results demonstrate that the proposed scheme could achieve better performance in terms of robustness and visual quality. In the future, we will focus on extending the application field of the proposed framework, such as the utilization of our framework into audio and video carriers.

References

[1] Y. Q. Shi, X. Li, X. Zhang, H. Wu, B. Ma, "Reversible data hiding: Advances in the past two decades," *IEEE Access*, vol. 4, pp. 3210–3237, 2016. Article (CrossRef Link)

[2] M. Goljan, J. Fridrich, R. Du, "Distortion-free data embedding for images," in *Proc. of International Workshop on Information Hiding*, pp. 27–41, 2001. Article (CrossRef Link)

[3] M. U. Celik, G. Sharma, A. M. Tekalp, E. Saber, "Lossless generalized-lsb data embedding," *IEEE Transactions on Image Processing*, vol. 14, no. 2, pp. 253–266, 2005. Article (CrossRef Link)

[4] Z. Ni, Y. Q. Shi, N. Ansari, W. Su, "Reversible data hiding," *IEEE Transactions on Circuits and Systems for Video Technology*, vol. 16, no. 3, pp. 354-362, March 2006. Article (CrossRef Link)

[5] X. Gao, L. An, Y. Yuan, D. Tao, X. Li, "Lossless data embedding using generalized statistical quantity histogram," *IEEE Transactions on Circuits and Systems for Video Technology*, vol. 21, no. 8, pp. 1061–1070, Aug. 2011. Article (CrossRef Link)

[6] C. Dragoi, D. Coltuc, "Improved rhombus interpolation for reversible watermarking by difference expansion," in *Proc. of the 20th European Signal Processing Conference (EUSIPCO)*, pp. 1688–1692, 2012. Article (CrossRef Link)

[7] X. Li, B. Li, B. Yang, T. Zeng, "General framework to histogram shifting-based reversible data hiding," *IEEE Transactions on Image Processing*, vol. 22, no. 6, pp. 2181–2191, June 2013. Article (CrossRef Link)

[8] X. Wu, J. Weng, W. Yan, "Adopting secret sharing for reversible data hiding in encrypted images," *Signal Process.*, vol. 143, pp. 269–281, 2018. Article (CrossRef Link)

[9] J. Wang, J. Ni, X. Zhang, Y. Q. Shi, "Rate and Distortion Optimization for Reversible Data Hiding Using Multiple Histogram Shifting," *IEEE Transactions on Cybernetics*, vol. 47, no. 2, pp. 315–326, Feb. 2017. Article (CrossRef Link)

[10] J. Tian, "Reversible data embedding using a difference expansion," *IEEE Transactions on Circuits and Systems for Video Technology*, vol. 13, no. 8, pp. 890–896, Aug. 2003. Article (CrossRef Link)
[11] I. Dragoi, D. Coltuc, "Local-prediction-based difference expansion reversible watermarking," *IEEE Transactions on Image Processing*, vol. 23, no. 4, pp. 1779-1790, April 2014. Article (CrossRef Link)
[12] S. Weng, Y. Chen, W. Hong, J. Pan, C. Chang, Y. Liu, "An improved integer transform combining with an irregular block partition," *Symmetry*, vol. 11, no. 1, p. 49, 2019. Article (CrossRef Link)
[13] D. Coltuc, "Improved embedding for prediction-based reversible watermarking," *IEEE Transactions on Information Forensics and Security*, vol. 6, no. 3, pp. 873–882, Sep. 2011. Article (CrossRef Link)
[14] X. Li, B. Yang, T. Zeng, "Efficient reversible watermarking based on adaptive prediction-error expansion and pixel selection," *IEEE Transactions on Image Processing*, vol. 20, no. 12, pp. 3524-3533, Dec. 2011. Article (CrossRef Link)
[15] I. C. Dragoi, D. Coltuc, "On local prediction based reversible watermarking," *IEEE Transactions on Image Processing*, vol. 24, no. 4, pp. 1244–1246, April 2015. Article (CrossRef Link)
[16] I. Dragoi, D. Coltuc, "Adaptive pairing reversible watermarking," *IEEE Transactions on Image Processing*, vol. 25, no. 5, pp. 2420–2422, May 2016. Article (CrossRef Link)
[17] Y. Ke, M. Zhang, J. Liu, T. Su, and X. Yang, "Fully Homomorphic Encryption Encapsulated Difference Expansion for Reversible Data Hiding in Encrypted Domain," *IEEE Transactions on Circuits and Systems for Video Technology*, vol. 30, pp. 2353-2365, Aug. 2020. Article (CrossRef Link)
[18] L. Xiong, D. Dong, "Reversible data hiding in encrypted images with somewhat homomorphic encryption based on sorting block-level prediction-error expansion," *Journal of Information Security and Applications*, vol. 47, pp. 78-85, 2019. Article (CrossRef Link)
[19] C.C. Chang, T.D. Kieu, Y.C. Chou, "Reversible data hiding scheme using two steganographic images," in *Proc. of IEEE Region 10 International Conference (TENCON)*, pp. 1–4, 2007. Article (CrossRef Link)
[20] C.C. Chang, T.C. Lu, G. Hong, Y.H. Huang, Y.M. Hsu, "A high payload data embedding scheme using dual stego-images with reversibility," in *Proc. of the 9th International Conference on Information, Communications & Signal Processing*, pp. 1–5, 2013. Article (CrossRef Link)
[21] T.C. Lu, J.H. Wu, C.C. Huang, "Dual-image-based reversible data hiding method using center folding strategy," *Signal Process*, vol. 115, pp. 195–213, 2015. Article (CrossRef Link)
[22] T.C. Lu, H.S. Leng, "Reversible dual-image-based hiding scheme using block folding technique," *Symmetry*, vol. 9, no. 10, p. 223, 2017. Article (CrossRef Link)
[23] T.C. Lu, C.Y. Tseng, J.H. Wu, "Dual imaging-based reversible data hiding technique using LSB matching," *Signal Process*, vol. 108, pp. 77–89, 2015. Article (CrossRef Link)
[24] I.F. Jafar, K.A. Darabkh, R.T. Al-Zubi, R.R. Saifan, "An efficient reversible data hiding algorithm using two steganographic images," *Signal Process*, vol. 128, pp. 98–109, 2016. Article (CrossRef Link)
[25] H. Yao, F.Y. Mao, Z.J. Tang, C. Qin, "High-fidelity dual-image reversible data hiding via prediction-error shift," *Signal Processing*, vol. 170, p. 107447, 2020, Article (CrossRef Link)
[26] X. Jin, L. Su, J. Huang, "A reversible data hiding algorithm based on secret sharing," *Journal of Information Hiding and Privacy Protection*, vol.3, no.2, pp. 69–82, 2021. Article (CrossRef Link)
[27] J. Liu, R. Zhang, J. Li, L. Guan, C. Jie, J.P. Gui, "A reversible data hiding algorithm based on image camouflage and bit-plane compression," *Computers, Materials & Continua*, vol. 68, no.2, pp. 2633–2649, 2021. Article (CrossRef Link)
[28] Z.X. Yin, Y.Z. Xiang, X.P. Zhang, "Reversible Data Hiding in Encrypted Images Based on multi-MSB Prediction and Huffman Coding," *IEEE Transactions on Multimedia*, vol. 22, no. 4, pp. 874-884, April 2020. Article (CrossRef Link)
[29] C. Qin, W. Zhang, F. Cao, X. P. Zhang, and C.-C. Chang, "Separable Reversible Data Hiding in Encrypted Images via Adaptive Embedding Strategy with Block Selection," *Signal Processing*, vol. 153, pp. 109–122, 2018. Article (CrossRef Link)

[30] C. D. Vleeschouwer, J. F. Delaigle, B. Macq, "Circular interpretation of bijective transformations in lossless watermarking for media asset management," *IEEE Trans. Multimedia*, vol. 5, no. 1, pp. 97–105, Mar. 2003. Article (CrossRef Link)
[31] Z. Ni, Y. Q. Shi, N. Ansari, W. Su, Q. Sun, X. Lin, "Robust lossless image data hiding designed for semi-fragile image authentication," *IEEE Transactions on Circuits and Systems for Video Technology*, vol. 18, no. 4, pp. 497–509, Apr. 2008. Article (CrossRef Link)
[32] X.T. Zeng, L.D. Ping, X.Z. Pan, "A lossless robust data hiding scheme," *Pattern Recognit.*, vol. 43, no. 4, pp. 1656–1667, Apr. 2010. Article (CrossRef Link)
[33] X. Gao, L. An, Y. Yuan, D. Tao, X. Li, "Lossless data embedding using generalized statistical quantity histogram," *IEEE Transactions on Circuits and Systems for Video Technology*, vol. 21, no. 8, pp. 1061–1070, Aug. 2011. Article (CrossRef Link)
[34] X. Liu, J. Lou, H. Fang, Y. Chen, P. Ouyang, Y. Wang, B. Zou, L. Wang, "A novel robust reversible watermarking scheme for protecting authenticity and integrity of medical images," *IEEE Access*, vol. 7, pp. 76580–76598, 2019. Article (CrossRef Link)
[35] D. Coltuc, "Towards distortion-free robust image authentication," *J. Phys., Conf. Ser.*, vol. 77, no. 1, p. 012005, Jul. 2007. Article (CrossRef Link)
[36] D. Coltuc, J.-M. Chassery, "Distortion-free robust watermarking: A case study," in *Proc. of SPIE*, vol. 6505, pp. 585-592, Feb. 2007. Article (CrossRef Link)
[37] R. Hu, S. Xiang, "Cover-Lossless Robust Image Watermarking Against Geometric Deformations," *IEEE Transactions on Image Processing*, vol. 30, pp. 318-331, 2021. Article (CrossRef Link)
[38] L. An, X. Gao, X. Li, D. Tao, C. Deng, J. Li, "Robust reversible watermarking via clustering and enhanced pixel-wise masking," *IEEE Transactions on Image Process.*, vol. 21, no. 8, pp. 3598–3611, Aug. 2012. Article (CrossRef Link)
[39] R.W. Hu, S.J. Xiang, "Lossless robust image watermarking by using polar harmonic transform," *Signal Processing*, vol. 179, p. 107833, 2021. Article (CrossRef Link)
[40] X. Wang, X. Li, Q. Pei, "Independent embedding domain based two stage robust reversible watermarking," *IEEE Transactions on Circuits and Systems for Video Technology*, vol. 30, no. 8, pp. 2406-2417, Aug. 2020. Article (CrossRef Link)
[41] R. Thabit, B.E. Khoo, "A New Robust Reversible Watermarking Method in the Transform Domain," in *Proc. of The 8th International Conference on Robotic, Vision, Signal Processing & Power Applications. Lecture Notes in Electrical Engineering*, vol. 291, pp. 161–168 2014. Article (CrossRef Link)
[42] L. Xiong, X. Han, C.N. Yang, Y.Q. Shi, "Robust Reversible Watermarking in Encrypted Image with Secure Multi-party based on Lightweight Cryptography," *IEEE Transactions on Circuits and Systems for Video Technology*, vol. 32, no. 1, pp. 75-91, Jan. 2022. Article (CrossRef Link)
[43] S.W. Byun, H.S. Son and S.P. Lee, "Fast and Robust Watermarking Method Based on DCT Specific Location," *IEEE Access*, vol. 7, pp. 100706-100718, 2019. Article (CrossRef Link)
[44] CVG-UGR databases. [Online]. Available: https://decsai.ugr.es/cvg/dbimagenes/index.php
[45] DIP databases. [Online]. Available: http://www.imageprocessingplace.com

Xuejing Guo received the B.S. degree from the Jingdezhen Ceramic Institute, Jiangxi, China, in 2018, where he is currently pursuing the M.S. degree with the School of Mechanical and Electronic Engineering. His current research interests include digital watermarking and forensics.

Junxiang Wang received the M.S. degree from the Harbin Institute of Technology, Harbin, China, in 2008, and the Ph.D. degree from Sun Yat-sen University, Guangdong, China, in 2012. He has been a Visiting Scholar with the New Jersey Institute of Technology, Newark, NJ, USA, since 2017. He is currently a Professor with the School of Mechanical and Electronic Engineering, Jingdezhen Ceramic Institute, Jiangxi, China. His current research interests include information security and image processing.

Yixiang Fang eceived the B.Sc. degree from Harbin Institute of Technology, China, in 2009 and the M.S. degree in 2012. And he has been with the faculty of the School of Mechanical and Electronic Engineering, Jingdezhen Ceramic Institute. His current research interests include privacy preservation information hiding, digital forensics and multimedia security.

Wenchao Zeng received the B.S. degree from the Jingdezhen Ceramic Institute, Jiangxi, China,in 2019, where he is currently pursuing the M.S. degree with the School of Mechanical and Electronic Engineering. His current research interests include digital watermarking and forensics.

Yi Zhao received an M.S. degree from the Guilin University of electronic technology, Guangxi, China, in 2011. She is a lecturer at the School of Mechanical and Electronic Engineering, Jingdezhen Ceramic University, Jiangxi, China. Her current researches include information security and image processing.

Tianzhu Zhang received an M.S. degree from Nanchang University in 2019. He is an assistant teacher at the School of Mechanical and Electrical Engineering, Jingdezhen Ceramic University, Jiangxi China. His current research interests include information security and image processing and underground target detection.

Yunqing Shi received the M.S. degree from Shanghai Jiao Tong University, Shanghai, China, and the Ph.D. degree from the University of Pittsburgh, Pittsburgh, PA, USA. He has been with the NewJersey Institute of Technology, Newark, NJ, USA, since 1987. He has authored/coauthored 300 papers, one book, five book chapters, and an editor often books. He holds 28 U.S. patents. His current research interests include digital data hiding, forensics and information assurance, visual signal processing, and communications.